Comparison of the LEMUR and PSST Image Processing Pipelines for Astrometric Measurements of Resident Space Objects in All Orbital Regimes

Leonid Shakun[1], Krzysztof Kamiński[2], Oleksandr Briukhovetskyi[3], Justyna Gołębiewska[2], Edwin Wnuk[2], Monika K. Kamińska[2], Mikołaj Krużyński[2], Vadym Savanevych[4], Oleksandr Kozhukhov[5], Vladimir Vlasenko[5], Eugen Dikov[6], Artem Dmytrenko[7], Nikolay Koshkin[1]

[1] Astronomical Observatory, Odesa I.I.Mechnikov National University
[2] Astronomical Observatory Institute, Faculty of Physics, A. Mickiewicz University
[3] Western Radio Technical Surveillance Center, National Space Facilities Control and Test Center of State Space Agency of Ukraine
[4] Department of systems engineering Kharkiv National University of Radio Electronics
[5] National Space Facilities Control and Test Center of State Space Agency of Ukraine
[6] Research and Design Institute of Micrography
[7] Institute of Astronomy of V.N.Karazin Kharkiv National University

ABSTRACT

Today many observers use telescopes with small apertures and a wide field of view for space debris observations. They compensate for an image's low angular resolution using special image processing pipelines that allow measurements of satellite positions with subpixel accuracy. A typical way of identifying systematic measurement errors is to compare measurements with well-known orbits of reference objects. Unfortunately, this method usually does not allow to identify the origin of systematic errors. In this work we supplement the traditional way of comparing measurements of reference objects with a known orbit by comparing measurements between two independent implementations of image processing pipelines. This allows us to identify systematic errors associated with the implementation of a specific pipeline. In this work, we present the comparison of the Ukrainian LEMUR and Polish Poznań Satellite Software Tools (PSST) image processing pipelines.

The LEMUR and PSST pipelines can accurately process images from various equipment. Both tools measure resident space object (RSO) coordinates with subpixel accuracy (about 0.1 pixels). The single position measurement accuracy for objects on LEO is about one arcsecond; for objects on medium and high orbits, the accuracy is about a few tenths of an arcsecond. The accuracy of a single measurement of both pipelines depends on many factors and has significant variations depending on the image characteristics. We suppose that PSST better adapts to the complex point spread function, which allows PSST to produce more accurate measurements for complex images. The pipelines produce very similar results, but occasionally can produce measurements that may have significant systematic differences. In some cases, we have identified systematic variations in measurement residuals with respect to reference orbits that are similar in both pipelines. We suppose that these systematic variations are due to equipment work peculiarities. We found that the systematic differences between both pipelines are usually lower than the systematic differences between measurements and reference orbits. Therefore, we conclude that the quality of results obtained by both pipelines is high, and the remaining residuals are worth investigating. We suppose that specific systematic variations of our observations presented in the work are not unique, and our description can help other researchers better understand their observation results.

1. INTRODUCTION

As more and more space debris accumulate in orbit, accurate measurements of their positions become increasingly crucial for ensuring the safety of satellites and spacecrafts, especially in low Earth orbit (LEO) regime. One of the ways to observe space debris is through ground-based optical observations. Accurate orbit determination of resident space objects (RSOs) on Earth orbit based on optical observations requires the joint use of observations from many telescopes in different parts of the globe. However, due to differences in construction, observation methodology and image processing techniques, each telescope provides an observation quality that varies significantly. As a result, the orbit determination using joint observations requires estimating each telescope's observation quality. The traditional

procedure for assessing observation quality involves comparing an observation set with a well-known orbit of reference objects, which often reveals significant systematic differences between observations and prediction (O-C) based on the known orbit.

While the magnitude of random errors can easily be reduced by increasing the number of measurements, reducing the influence of systematic differences between station measurements can be achieved by increasing the number of observing stations, which is usually complex and sometimes impossible, or by measurement calibration. Therefore, the possibility of detecting, measuring, and subsequently reducing the magnitude of systematic measurement errors is of great interest for improving the accuracy of orbit estimation of RSOs.

Systematic differences in the O-Cs can be caused, among others, by

1) inaccuracy of the reference orbit,
2) systematic measurement errors in the object coordinates in the image,
3) and methodology inaccuracies in comparing measurements and a reference orbit.

Finding the original cause of systematic differences in O-Cs is challenging in practice. The first and third reasons introduce systematic differences in O-Cs during the comparison procedure and are inherently unrelated to the measuring procedure of the object coordinates. However, there is no clear way to separate the measurements' systematic biases from the comparison procedure's systematic biases.

The typical comparing procedure for the measurements and the reference orbit includes reduction of aberrations and correction of the systematic time biases of the measurements. In addition to these operations, we corrected the observation station location coordinates and the refraction parallax effect. We discuss more details of the comparison procedure in section 5. In analyzing systematic biases, we aim to identify cases where the orbital information is insufficiently accurate and exclude such data from the comparison procedure.

This work investigates the results of measuring RSO coordinates on the same observation sets using two image processing pipelines, the Ukrainian LEMUR and Polish Poznań Satellite Software Tools (PSST). We compare the differences between O-Cs from both pipelines with respect to the values of O-Cs.

In the following sections we present a brief description of both pipelines (sections 3 and 4), investigate differences in astrometric measurements produced by the LEMUR and PSST, study the residuals between observations and reference orbit and separate the systematic variations in measurements due to image processing methods from those due to equipment and observation process (section 5 and 6).

2. OBSERVATION EQUIPMENT

Poznań SST Telescope 3 (PST3) is a cluster of 5 optical telescopes located in Chalin Observing Station (western Poland) of Astronomical Observatory Institute of Adam Mickiewicz University [1]. During this study only two telescopes from the cluster were utilized. Their specification is given in Table 2.1.

Table 2.1: The PST3 and OEOS-3 specifications.

Parameter	PST3c	PST3e	OEOS-3/OES35
Aperture [mm]	318	300	350
Focal length [mm]	2541	300	700
Camera (Sensor)	Andor Zyla 5.5 + GPS	Andor Zyla 5.5 + GPS	QHY-174M GPS
Sensor size [pix]	2560 x 2160	2560 x 2160	1936x1216
Pixel size [µm]	6.5	6.5	5.86
Scale without binning ["/pix]	0.53	4.39	1.73
FoV [deg]	0.37° x 0.32°	3.2° x 2.7°	0.92° x 0.58°
Mount	Alt-Az with direct drive	Alt-Az with direct drive	Modified German with direct drive
Max. slew rate [deg/s]	50	50	20
Non-sidereal tracking	Yes	Yes	Yes

OES35 is a wide field of view (FoV) telescope, part of the two-tube Optical-Electronic Observation Station Type 3 (OEOS-3), located in western Ukraine, in the Zakarpatska region. Below are the main characteristics of the telescope, but a more detailed report was given at AMOS-2022 [2]. The specifications of the telescope are presented in Table 2.1.

3. PSST

Poznań Satellite Software Tools (PSST) is a collection of programs and scripts dedicated for astrometric and photometric analysis of optical observations of artificial Earth orbiting objects. The package has been in development since 2016 and is in regular use at several telescopes since 2019. From the beginning the main idea was to be able to process even significantly elongated and deformed satellite or stellar trails and to be able to integrate the package, or its components, with automatic reduction pipelines. For that reason, the software has no GUI and is controlled by command line options or configuration files. PSST data processing steps comprise of the following main steps: data preparation, image analysis, astrometry and photometry, target identification, quality control.

1. During data preparation images are prepared for analysis by performing standard image reduction with calibration frames. For telescopes in which image timing is collected in a separate text file, by an external GPS timer connected to a camera, FITS headers are also updated with the correct timing information.
2. The purpose of image analysis step is to convert 2D pixel data into a list of objects. For that to happen image background is measured by calculating medians of pixel values in a grid of small image subsections. These values are then interpolated and used to flatten the image. Then the image is optionally smoothed, and a threshold ADU level is calculated using statistics of the background pixels. Pixel groups above the threshold, regardless of their shape, are considered candidates for objects in the image. Candidates are checked for compliance with user selected requirements such as minimum number of pixels, object elongation or size limit, etc. For accepted objects their location in the image (centroid), shape (elongation), brightness and other characteristics are saved for subsequent analysis.

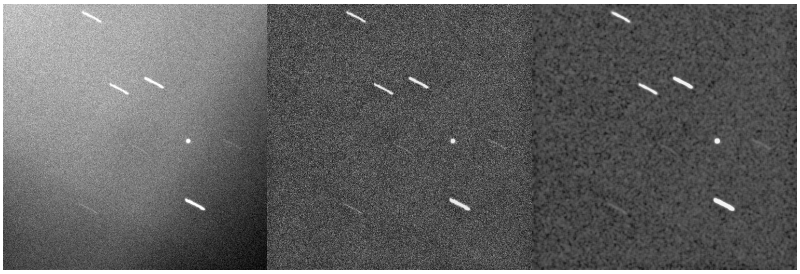

Fig 3.1. From left: image after reduction, image with flattened background, image after blurring to emphasize dim objects.

Fig 3.2. From left: image prior to object extraction, pixels above threshold value, selected pixel groups after filtering, raw image with centroid positions (red circles) of selected pixel groups overplotted.

3. Using the positions of all objects found in the image and the Gaia DR3 stellar catalog, a subset of these objects is identified as stars. Depending on the number of reference stars an astrometric transformation of the order of 1, 2 or 3 is constructed and applied to all objects in the image. The difference between calculated and catalog positions and magnitudes of stars are used to evaluate the precision of astrometry and photometry. Using all identified stars as a single reference "super-star" photometric magnitude is also calculated for each object in the image.
4. Depending on the type of observations (tracking or survey) the next step determines whether there are any objects which are stationary or linearly moving in the field of view of the telescope. This is done by

comparison of pixel positions of all objects in all images taken during a single image series. Optional drifting of the target in the image can be allowed and additional selection criteria can be applied here. Each accepted set of associated astrometric and photometric measurements in a single image series is considered a candidate for an Earth orbiting object. The astrometry of such candidate is compared with ephemeris of all known satellites in all images to identify the target. A threshold for astrometric error can be set by the user and is scaled with the distance of the object during observations.

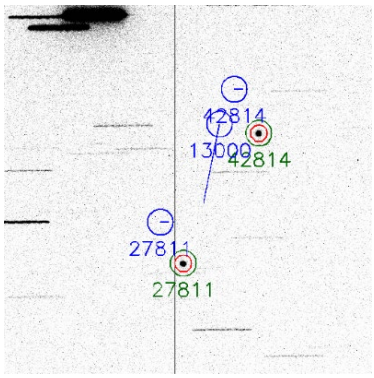

Fig. 3.3. Identification of two GEO satellites (green and red circles) based on the ephemeris using Space Track orbits. Blue circles and lines represent predicted positions and motions of three satellites in the FoV of the telescope. NORAD ID numbers are also presented.

5. The final step of the analysis is composed of filtering the measurements of observed artificial Earth satellite(s) based on the estimated quality of astrometry or other, user selected criteria. The final results are then saved in several formats, including CCSDS Tracking Data Message version 2.0. The software also generates several control images, presenting intermediate steps and final results, that can be inspected by the user.

4. LEMUR

The LEMUR software system started in 2008 as a graduate student project for processing astronomical images of spacecraft and small bodies of the Solar System. From the beginning it was clear that the concept of respected and proven programs, such as Astrometrica, in which the main labor input of the observer was spent on monotonous repeat of the same operations: load a series of frames - process (get a list of images/identify) a series of frames - mark satellites/asteroids on a series of frames - generate a report - repeat 50-100 times (according to the number of satellites, series, ...) was inadequate for working with large datasets. Understanding this the project set its goal to create a program with a high level of automation of solving the problem of detecting moving objects on a series of astronomical frames. LEMUR is implemented on the principle of client-server architecture, where the server part is represented by parallelized clones, each of which processes a newly arrived frame. The client part is responsible for constant search of new frames on the user's computer, their validation, sending frames to the server, downloading already processed frames and found space objects from the server, generating reports with measurements (in different formats), setting processing parameters. This approach allows to have one dedicated server for processing, which is convenient for observatories that have, for example, more than one telescope, or for a distributed network of observers whose telescopes are located in different parts of the world.

Frame processing procedure of the LEMUR server.

1. Brightness equalization of the frame. It is known that not all observers use flat-frames, especially when conducting satellite surveys, where hundreds and thousands of frames can be created. Moreover, observations might be conducted at low altitudes and possibly influenced by stray light. In such conditions the use of flat-frames might not always be reasonable and sometimes harmful. This problem is solved by an embedded mathematical low-pass filter implemented on the basis of an inverse median filter. We have conducted studies [3] which have shown that the filter realized by us does not distort the brightness of high frequencies, which preserves the scientific (photometric) value of the obtained images.

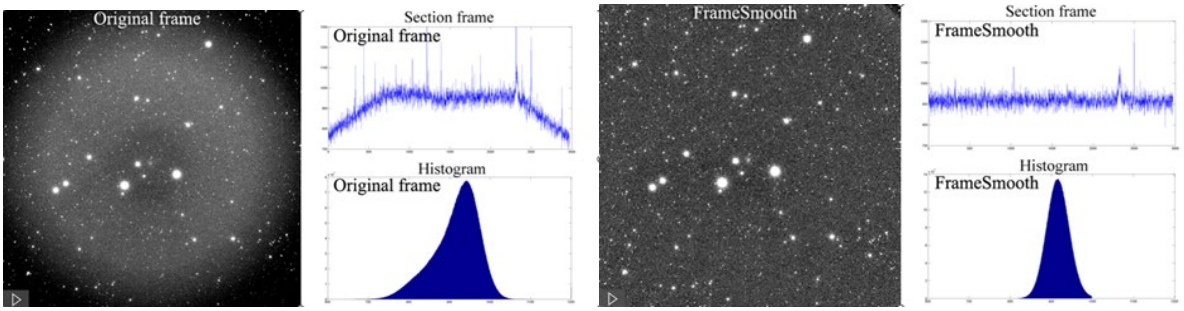

Fig. 4.1 Example of brightness equalization of frames

2. Identify the type of frame: are the images of stars in the frame represented by points or streaks? The observation of RSOs can be carried out with different telescope modes, so that the images of stars can become blurred (streaks) or be point-like (in the case of sidereal tracking or super short exposures). Since star images are the main type of images in the frame, from the point of view of application of the most appropriate computational methods of image detection and minimization of computational costs, it is reasonable to determine the shape of star images in advance. In the program this function is implemented on the basis of analysis of the modulus of the frame spectrum.
During the transition from the spatial to the frequency domain, the signs of synchronous elongation of all objects are accumulated, and the elongation of the images of the frame objects is characterized by one single sign - the elongation of the spectrum module image. As a degree of elongation of the object image the estimation of its eccentricity is used. The value of eccentricity varies from 0 to 1. It is equal to 0 if the image of the object spectrum module has the shape of a circle and to 1 for the image of the spectrum module in the shape of a line.

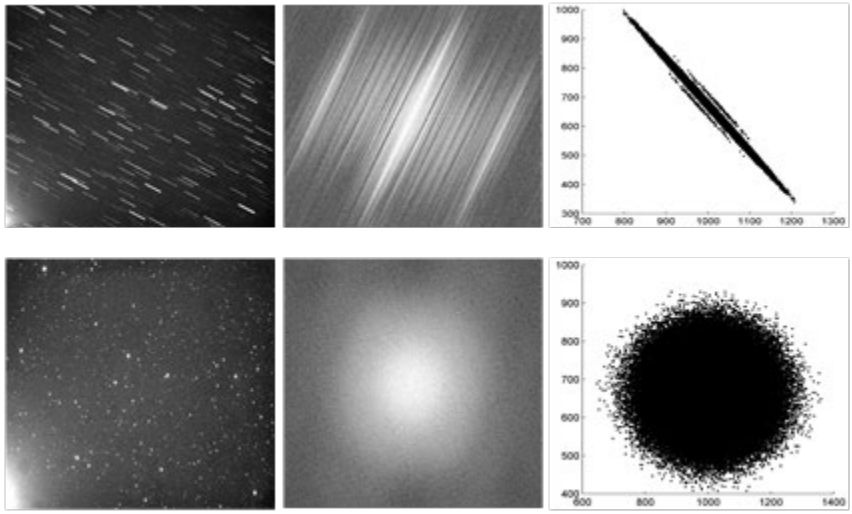

Fig. 4.2 Example of spectra of different types of images

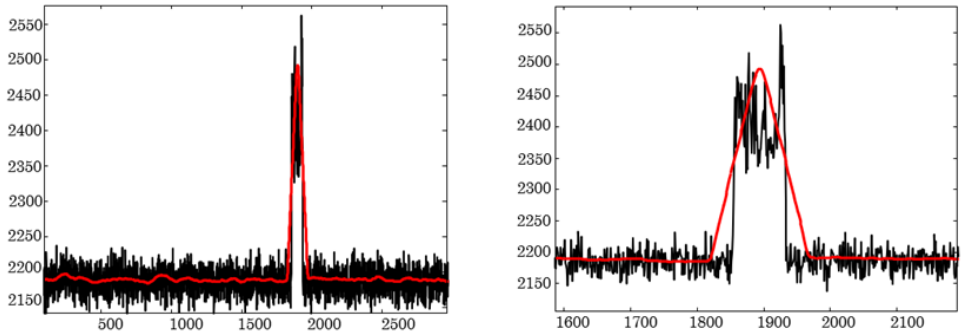

Fig. 4.3 Example of matched filter operation

3. Detection of images of space objects in the frame. If we set ourselves the task of automatic detection of moving objects in a series of frames, then the question of detection of faint images in a frame arises. The main source of interference (false detections) in frames with star streaks are parts (fragments) of faint stars, which were not grouped into one set of pixels, but form many separate detections. We found a solution to this problem in the application of a matched filter of two kinds - with an analytically specified profile and a typical image with an analytically unspecified profile.

In the first case, the transfer characteristic of the matched filter is determined by the type of analytical model of the smeared image of objects with known parameters. Blurred images of objects are represented by a set of Gaussians. According to the model used in this paper, the centers of the Gaussians lie on one straight line passing through the point of the center of reference of the blurred image of the j-th object with coordinates $x_{\tau j}$ ($\Theta_{\tau j}^{over}$) and $y_{\tau j}$ ($\Theta_{\tau j}^{over}$) at an angle ω_j to the abscissa axis in the digital frame coordinate system.

For the variety of object images encountered in different digital frames, the use of an analytical model is not always justified. Due to inaccuracies of tracking or wind gusts the typical shape of object images changes from frame to frame (Fig. 4.4). Taking into account all random factors affecting the shape of the object image in the analytical model leads to its complication and increases the number of model parameters, which leads to high computational costs and decreased accuracy of the model parameters estimation.

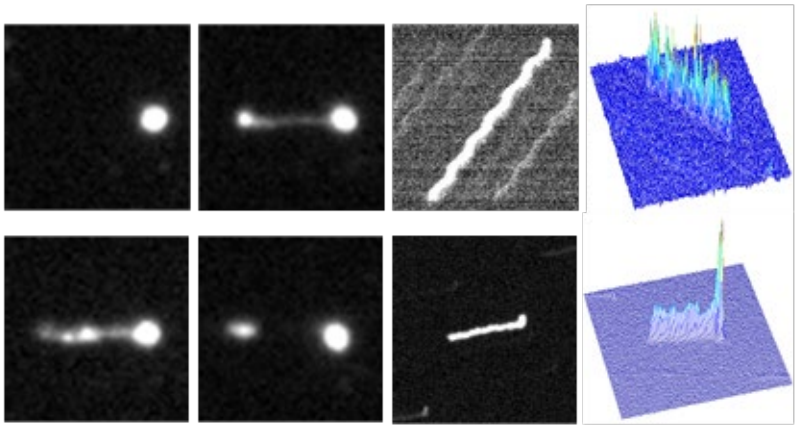

Fig. 4.4 Examples of blurred images of objects on a series of digital frames: errors in sidereal tracking, inaccuracies of spacecraft tracking, wind gusts.

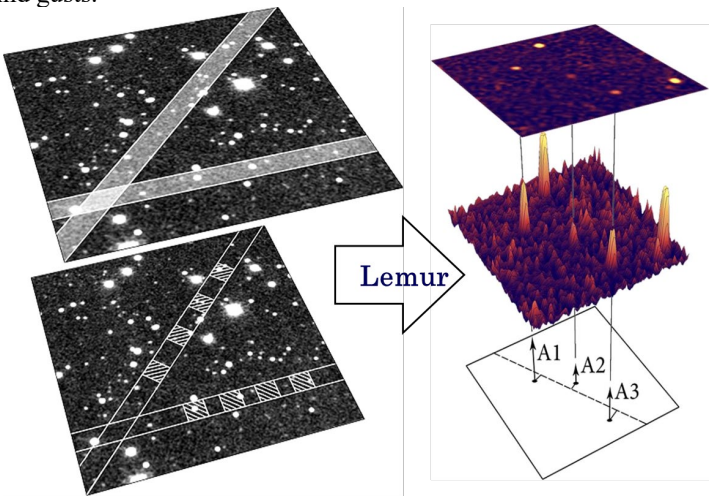

Fig. 4.5 Schematic representation of the operation of the method of statistics accumulation along a trajectory which parameters are not known.

In order to simplify the estimation of the transfer characteristic of the matched filter, it is proposed to use a typical image in a frame corresponding to the average image of objects as a model of all object images. In this case, the type of object image, its shape, brightness distribution in the object image will be determined only by the typical image.

4. Detection of moving objects. After completion of in-frame processing of all frames (formation and classification of the list of images, astrometric and photometric analysis) searching for moving objects begins. It consists of several computational methods, such as the strobe method and the method of accumulation of statistics along the trajectory, the parameters of which are not known. The moving object detection procedures select measurements that have not been identified with star catalogs, are not anomalous pixels and are not stationary objects in a series of frames. The combination of the implemented methods allows the LEMUR program to detect satellites in all types of orbits – LEO, MEO, GEO.

5. Visual control of the processing result and report with measurements. After completion of all processing stages, the observer can load processed frames with detected objects, view the processing results, and generate measurement reports.

5. METHODOLOGY

The comparison of optical astrometric observations of an RSO with precise reference orbits is the typical method for studying their quality. Precise reference orbits are usually provided in the form of orbital products from services such as the International Laser Ranging System (ILRS), Doppler Orbitography and Radiopositioning Integrated by Satellite (DORIS), and the International GNSS Service (IGS).

A typical procedure for analyzing the quality of observations includes the following steps [4, 5, 6]:

1) Correcting aberrations of the measured celestial equatorial coordinates of RSO.
2) Correcting the systematic time bias of all measurements.
3) Calculating O-Cs in the celestial equatorial coordinates system.

The typical criterion of measurement quality is the root mean square deviation (RMSD) of O-Cs, the number of detected gross measurement errors and the magnitude and invariability of the time bias of the measurement series. This approach considers any deviation from the orbital prediction as a random error that we can describe by the RMSD value of a single measurement.

Fig. 5.1 shows, as an example, the result of such a comparison for the low-orbit object Jason-3. The residuals clearly show systematic trends which have complex and incomprehensible behavior. Indeed, the O-Cs presented in the equatorial coordinate system do not have a clear relation to the reasons of the systematic errors and will manifest differently in different sets of observations.

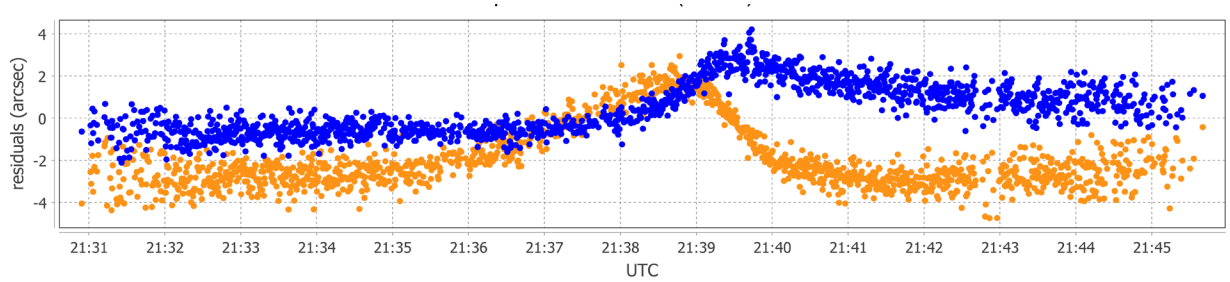

Fig. 5.1 – An example of the O-C in the form of equatorial coordinates with respect to the reference orbit provided by DORIS for the Jason-3 (NORAD: 41240) on March 19, 2022. Observations were obtained at the PST3 station in Chalin (Poland). Blue points are right ascension residuals (multiplied by the cosine of declination). Orange points are declination residuals.

We prefer to consider the O-Cs in a decomposition form of the residual vector along the object's visible trail on the celestial sphere (L-component of O-C) and across the visible trail (N-component of O-C). This decomposition has several obvious advantages over representing O-Cs in equatorial coordinates.

The elongated images of stars or tracked object (dependent on the observation mode) lead to non-equivalent measurement random error properties along and across the visible trail. The covariance matrix that describes error

properties in the equatorial coordinate system will depend on time, even if fundamental error properties along and across the visible trail are constant. If we expect that fundamental error properties along and across the visible trail are stable, then the O-C statistical properties in the LN-decomposition are more useful in the studying measurement quality. The O-Cs along and across the visible trail are also devoid of nonlinearities that are inherent in the residuals in equatorial coordinates.

The errors in registering the time moments introduce proportional measurement errors along the visible trail and only indirectly affect the errors across the visible trail. For each separate measurement, we can recalculate the along the visible trail O-C value in terms of time delay (we call this T-component of the O-C).

Given that the angular resolution of the telescope on which the original images were obtained is 9”/pix, the implementation specifics of the image processing pipeline might be the cause of the systematic trends visible in Fig. 5.1. As we will show in section 6, image processing programs can indeed measure object coordinates with a systematic bias. However, the magnitude of this bias rarely exceeds 1 arcsecond for low-orbit objects. Therefore, this cannot explain all aspects of observed systematic deviations in O-Cs.

Other factors, besides measurement errors, that can cause systematic trends in O-Cs, which are usually neglected when comparing measurements and the reference orbit, are

1) the prediction inaccuracy of the reference object's position,
2) the error in the telescope coordinates obtained from the GPS receiver,
3) and the neglect of the refractive parallax effect [7].

A retrospective comparison of different ILRS predictions (in those cases when possible) shows that the difference in the predicted object's position is in the range from 1 to 100 meters. The amplitude of the detected differences in the predicted object's position varies significantly for different objects [8]. Therefore, when considering the measurement residuals, it is always necessary to consider the possible inaccuracies of the ILRS predictions.

However, the detected differences in the object's position predictions in most cases cannot explain the magnitude of the systematic trends in the O-Cs that we observe. Therefore, for our comparison, we estimated the telescope coordinates using the observations themselves. To this purpose, we solved the least square problem for the station coordinate fitting by minimizing the sum of the squares of the N-components of O-Cs (reference orbits were provided by DORIS). The correction values to the GPS coordinates of the observation sites are given in Table 5.1. For the coordinate estimation of the PST3 station, measurements obtained using the PSST pipeline were used, and for the coordinate estimation of the OES35 telescope, those obtained using the LEMUR pipeline were used. We used a significantly larger observation set to estimate the OES35 telescope coordinates than the one used for O-C analysis in this work (column 5 in Table 5.1). The observation set used to estimate the PST3 station coordinates is the same as the observation set used for O-C analysis in this work. We simultaneously used several objects supported by the DORIS service to estimate the observation site coordinates.

Table 5.1 – The correction values to the observation site GPS coordinates and the number of spacecraft passages that were used to estimate them.

Site	Longitude (deg)	Latitude (deg)	Altitude (m)	Number of spacecraft passages
PST3	-0.000083	0.000079	38.2	7
OES35	0.000026	0.000036	26.7	59

When calculating the O-Cs, we also consider the refraction parallax effect as a telescope position displacement in altitude above horizon. For this work, we calculated the telescope displacement due to refraction parallax using an exponential model of the Earth's atmosphere. We compared the telescope displacement based on our implementation of the refraction parallax effect and the displacement in accordance with the work [7]. In all cases we considered, the differences in the station displacement between our implementation and the implementation of [7] did not exceed 10% of the station displacement. We believe that these differences are acceptable within the framework of this work and plan to implement the refraction parallax model [7] for further research later.

Fig. 5.2 compares O-Cs for the Jason-3 (This observation set is the same observation set as shown in Fig. 5.1) in the case of using the GPS coordinates of the observation station and after their correction. We see that the coordinates correction of the observation site significantly reduced the systematic trends in the O-Cs. Importantly, in the example

presented here, the correction of the observation site coordinates eliminated the trend in the L-component of the O-Cs, which we did not use to correct the observation site location.

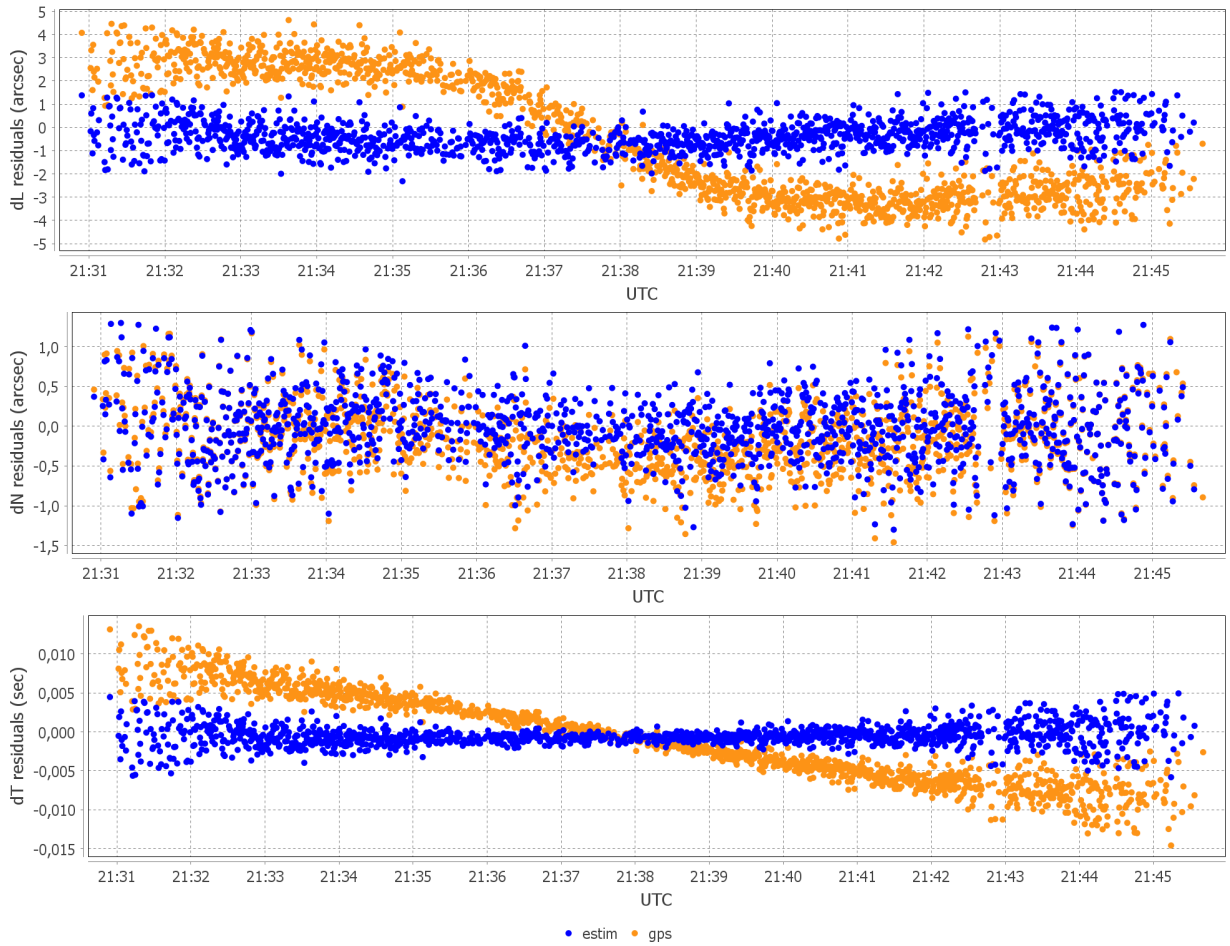

Fig. 5.2 – The comparison of the O-Cs for two variants of the observation station location. Each figure shows one of the components (L, N, or T) of the O-Cs. The orange points show the O-Cs calculated using GPS coordinates, and the blue points show the O-Cs calculated using the corrected coordinates of the observation station.

All calculations in this work were performed using the Korbest library [9] that we are developing. The Korbest library uses the OREKIT library [10] for orbit propagation and precision system coordinate transformations in 3D space. The code JSOFA [11] is used to calculate the annual aberration. The Korbest library implements the code for measurement objects and methods for evaluating model parameters, which differs from OREKIT. Among other things, Korbest allows decomposing the O-Cs vector into components along and across the object's visible trail and using this decomposition during orbit estimation, observation station coordinates correction, etc., which is impossible when using OREKIT to solve similar problems.

6. COMPARISON

We compare the measurement results of the PSST and LEMUR pipelines for the same observation sets. The observations were obtained during several consecutive observation campaigns in 2022 and 2023.

Depending on the orbit altitude, the apparent angular velocity of RSOs changes significantly. As a result, slightly different image processing and observation methods are usually used for LEOs and objects on higher orbits. The fast focal ratio telescope PST3e (f/1.0) with low angular image resolution (9"/pix) was used to obtain observations of objects with an orbital altitude below 6000 km, while PST3c with higher focal ratio (f/5.3) and a larger angular image resolution (2.1"/pix) was used to observe objects with orbital altitudes of more than 6000 km. At the OEOS-3 station,

we used the OES35 telescope with a focal ratio of f/2.0 and an angular image resolution of 1.73"/pix (Table 2.1) to observe all objects. As a result, diverse observation sets were obtained (Table 6.1).

No single service could provide reference orbital ephemerides for all objects considered in the study. Therefore, we used orbit products from one of the three services: ILRS, DORIS, and IGS, for each object (Table 6.1). In cases where we had a choice between several orbital ephemerides, we preferred those from DORIS and IGS. For the Starlette, LARES, and Lageos-1, only ILRS provides orbital ephemerides. We used orbital ephemerides from the 'product' section for these objects.

Table 6.1 – Summary of the observation sets and their corresponding reference orbits.

Orbit type	Telescope	Object name	NORAD ID	Number of frames	Number of measurements by PSST/LEMUR	Observation series count	Orbit product service (provider code)
LEO	PST3e	Starlette	07646	5000	4268 / 3610	5	ILRS product (NSGF)
		LARES	38077	2871	1502 / 1512	3	
		Jason-3	41240	8300	5111 / 5409	4	DORIS (CNES)
		SARAL	39086	1220	683 / 566	1	
		Sentinel-6A	46984	2500	2298 / 2378	2	
	OES35	Cryosat-2	36508	1680	696 / 1230	3	
		Jason-3	41240	1533	150 / 1220	2	
		Sentinel-6A	46984	1400	849 / 1339	2	
MEO	PST3e	Lageos-1	08820	4000	2548 / 1514	2	ILRS product (NSGF)
	PST3c	NAVSTAR	38833	8000	6044 / 7360	1	IGS (GFZ)
		NAVSTAR	39741	4952	1885 / 2758	1	
	OES35	NAVSTAR	43873	3000	2772 / 2929	1	
		NAVSTAR	46826	3000	1886 / 2895	1	
GSO	PST3c	Beidou-G5	38091	2000	685 / 1741	1	IGS (GFZ)
		IRNSS-1F	41384	2000	1540 / 1887	1	ILRS (ISR)
	OES35	Beidou-G5	38091	800	636 / 723	1	IGS (GFZ)
		IRNSS-1B	39635	800	582 / 742	1	ILRS (ISR)
		IRNSS-1F	41384	800	587 / 671	1	ILRS (ISR)

- NSGF – NERC Space Geodesy Facility (NSGF), formerly RGO, United Kingdom
- CNES – Centre National d'Etudes Spatiales (CNES), France
- GFZ – GFZ German Research Centre for Geosciences
- ISR – Indian Space Research Organization (ISRO)

6.1 LEO objects

Fig. 6.1 shows the statistical properties of O-Cs for measurements of the LEO objects made with the PST3e. The typical comparison using the RMS value (fig.6.1b) indicates PSST pipeline has approximately a 30% advantage in measurement accuracy over the LEMUR pipeline's measurements for L-components of the O-Cs and has no significant advantage in N-components of O-Cs. In Fig 6.1a, we can see that the means of the O-Cs (the bias of observation series) of the measurement series produced by the PSST and LEMUR pipelines are shifted against each other. LEMUR pipeline's measurements also show a slight systematic bias along the trail. We also note a scattering of the means of the O-Cs is around 1 arcsecond along and across the trail determined by reference orbit. The scattering amplitude is larger than the bias between the measurement results of the pipelines.

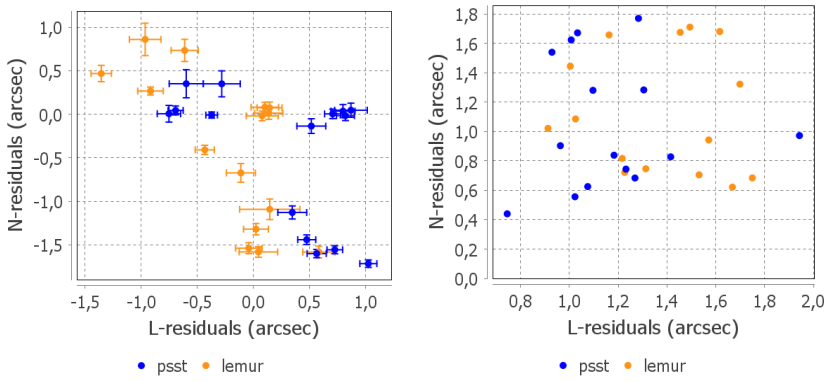

(a) (b)

Fig. 6.1 – Consolidated statistical properties of the O-Cs for measurements of the LEO objects at the PST3e telescope. (a) – the biases of the measurement series (mean values of the O-Cs) in the LN-decomposition of the O-Cs and 3σ-intervals for the mean values, (b) – RMSD of one measurement. Each point corresponds to one spacecraft passage. The blue points are PSST measurements, and the orange points are LEMUR measurements.

Fig. 6.2 shows the mean values of the O-Cs and the RMSD of the measurements only for the PSST pipeline. In Fig 6.2, we compare O-Cs using the reference orbits provided by the ILRS and DORIS services. It can be seen that the mean values of the O-Cs have a significantly lower scatter across the trail in the case of using the DORIS reference orbits than in the case of using the reference orbits provided by the ILRS service. We believe this is evidence of the insufficient accuracy of the ILRS orbital product for our study. Therefore, we decided to exclude from further consideration the objects Starlette and LARES, which are not supported by the DORIS service.

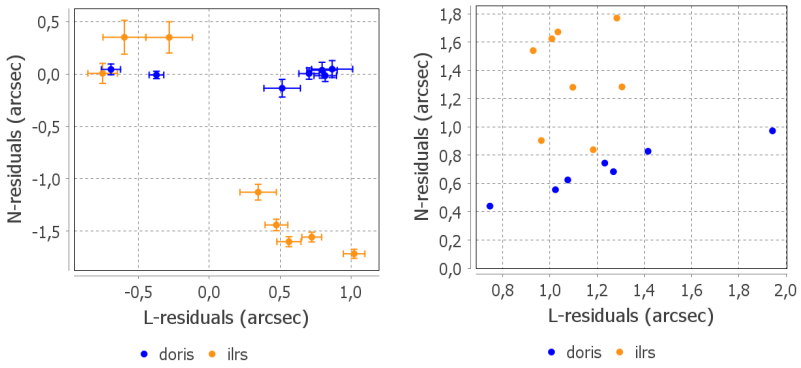

(a) (b)

Fig. 6.2 – Consolidated statistical properties of the O-Cs for measurements of LEO objects at the PST3e telescope. (a) – the mean values of the O-Cs in the LN-decomposition of the O-Cs and 3σ-intervals for the mean values, (b) – RMSD of one measurement. Each point corresponds to one spacecraft passage. The blue points are measurements in the case of using DORIS reference orbits, and the orange points are measurements in the case of using ILRS reference orbits.

Fig 6.3 shows only data for DORIS objects. Using more accurate orbital predictions makes it possible to identify that the PSST pipeline measurements have smaller series biases across the trail than the LEMUR measurements. Comparing Fig 6.3 with Fig 6.1, we see that the PSST pipeline measurements have a significantly smaller scatter of the mean values of O-Cs relative to DORIS orbits than the LEMUR pipeline measurements. This is most likely evidence of the high accuracy of PSST pipeline measurements across the trail. However, it should be kept in mind that the N-component residuals were used to estimate the PST3 station coordinates. Because the observation set is relatively small, it may lead to an underestimate of the scatter of the mean values of the O-Cs in the case of the PSST pipeline and PST3e telescope pair. The exclusion of ILRS orbits did not decrease the scatter of the series biases along the trail. From this, we conclude that the measurements probably contain time registration errors. The measurements in the green circles were obtained during one night on December 30, 2022, while the rest were on other dates. We see the excellent closeness of measurements for December 30, 2022, which probably indicates the stability of time registration moments over short intervals. Fig. 6.3c is equivalent to Fig. 6.1a, with only the difference that the series

biases along the trail are shown in time units. Thus, the uncertainty in the measurement registration moments in this observation set was about 1 ms.

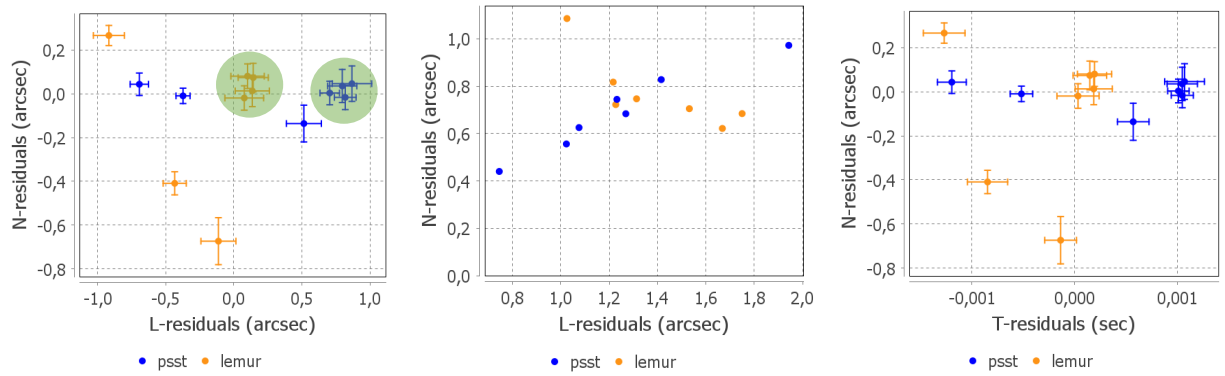

(a) (b) (c)

Fig. 6.3 – Consolidated statistical properties of the O-Cs for measurements of LEO objects at the PST3e telescope. (a) – the mean values of the O-Cs in the LN-decomposition of the O-Cs and 3σ-intervals for the mean values, (b) – RMSD of one measurement, (c) – the mean values of the O-Cs in the TN-decomposition of the O-Cs and 3σ-intervals for the mean values. Each point corresponds to one spacecraft passage. The blue points are PSST measurements, and the orange points are LEMUR measurements.

A more detailed analysis of the O-Cs in each separated spacecraft passage also reveals that the differences in the measurement results of the considered pipelines are not limited to only shifting all measurements in the passage by a fixed value (Fig. 6.4). In Fig. 6.4, we present one example of the passage in which the differences between the measurement results of the pipelines were most evident.

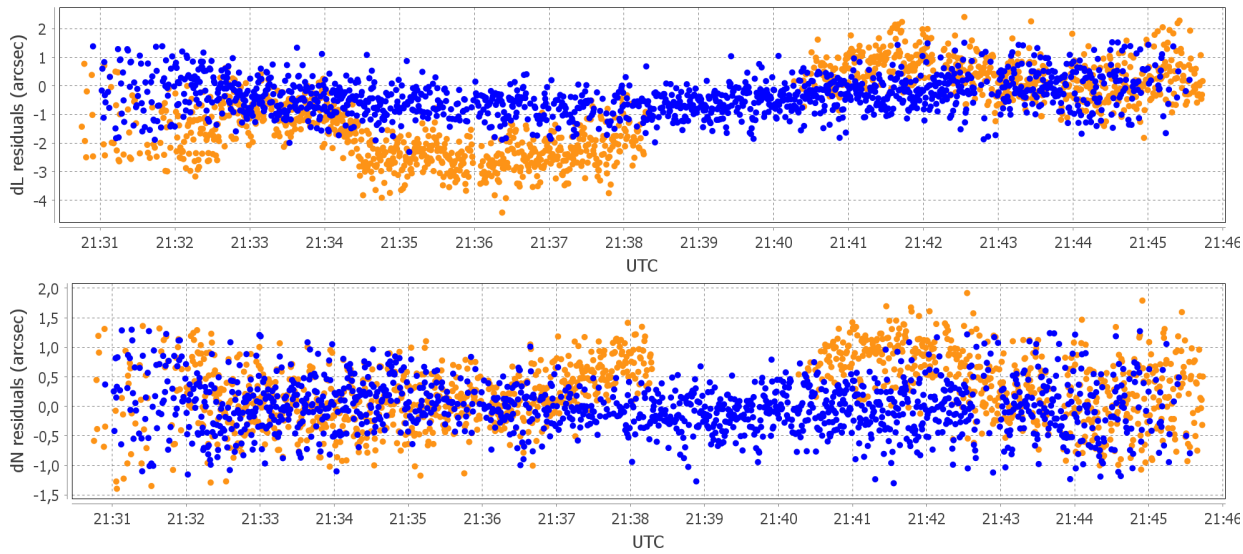

Fig. 6.4 – The comparison of the PSST and LEMUR O-Cs of object 41240 on the PST3e telescope on March 19, 2022. The blue points are the PSST O-Cs, and the orange points are the LEMUR O-Cs.

As we can see, the local differences between trends in the O-Cs of considered pipelines can reach 1 arcsecond, which is greater than the series biases we found for each spacecraft passage. Therefore, the scatter of series biases between the two pipelines in the case of short observation series can be even greater than shown in Fig. 6.1a. In our opinion, the significant and complex systematic differences between the pipelines were caused by the specificity of the source images. The PST3e telescope has a fast focal ratio optical system, which leads to significant image distortions. The results of our analysis show that the PSST pipeline is better than LEMUR at adapting to complex images with significant point spread function (PSF) distortions.

We also compared the PSST and LEMUR measurement results on a set of input images with fewer distortions, which were obtained on the OES35 telescope (Fig. 6.5). The comparison of both pipeline O-Cs in each spacecraft passage did not reveal significant trends between the PSST and LEMUR measurement results. It should also be noted that the PSST pipeline produced about half to two times fewer measurements than the LEMUR pipeline. Fig. 6.5b shows PSST measurements have a significantly lower magnitude of random error of one measurement across the trail than LEMUR. At the same time, LEMUR has a significantly lower magnitude of random error of one measurement along the trail than PSST.

Fig. 6.5a shows that all LEMUR measurements have a mean time bias of 0.5 ms and a small time dispersion, which displays the stability of the time registration system. PSST pipeline measurements have a larger time dispersion, so it is impossible to identify a time bias for them. However, we do not see a significant systematic bias between the LEMUR and PSST measurement groups (Fig. 6.5a). PSST pipeline measurements show fewer scatter of biases of observation series across the trail than LEMUR pipeline measurements. However, given the small data set, we consider these differences insignificant (Fig. 6.5a). Thus, pipelines can produce measurements with the significant bias of observation series (about several tenths of arcsecond) for the same passage. But when considering all measurement sets, there is no bias between PSST and LEMUR pipelines in the case of OES35 telescope images. Comparing Fig. 6.3 and 6.5, we can conclude that the LEMUR pipeline produces measurements with similar quality on both telescopes. The PSST pipeline on OES35 telescope images has a higher accuracy of one measurement across the trail than on PST3e images and a lower accuracy of one measurement along the trail.

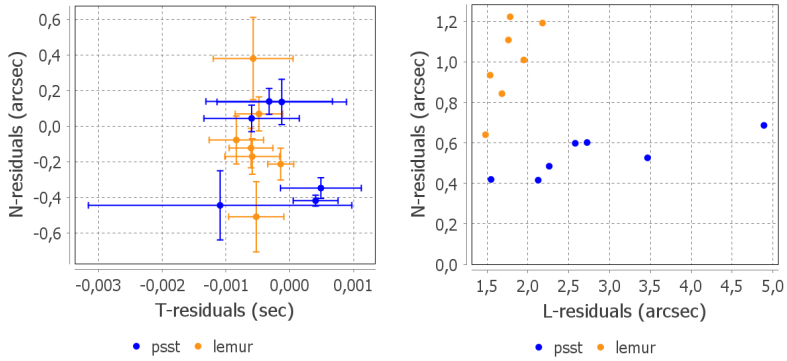

(a) (b)

Fig. 6.5 – Consolidated statistical properties of the O-Cs for measurements of the LEO objects at the OES35 telescope. (a) – the mean values of the O-Cs in the TN-decomposition of the O-Cs and 3σ-intervals for the mean values, (b) – RMSD of one measurement. Each point corresponds to one spacecraft passage. The blue points are PSST measurements, and the orange points are LEMUR measurements.

6.2 Lageos-1

Another interesting example of the non-random distribution of O-Cs was obtained for the Lageos-1 passage on August 3, 2022, on the PST3e telescope. Fig 6.6 shows clearly short-term systematic oscillations of the O-Cs for both L-component and N-component. These oscillations have an amplitude of about 1.5 arcseconds (in the case of the LEMUR pipeline, the amplitude is approximately 0.5 arcseconds larger) and are practically identical functions of time in the measurement results of both pipelines. The presence of oscillations in the N-component of the O-Cs excludes time registration problems from the list of the possible causes. The short-term nature of these oscillations also excludes the possibility of their occurrence due to inaccuracies in the orbital prediction. Therefore, the most likely cause of systematic measurement biases is the images' features, which finally lead to the displacement of consecutive groups of measurements.

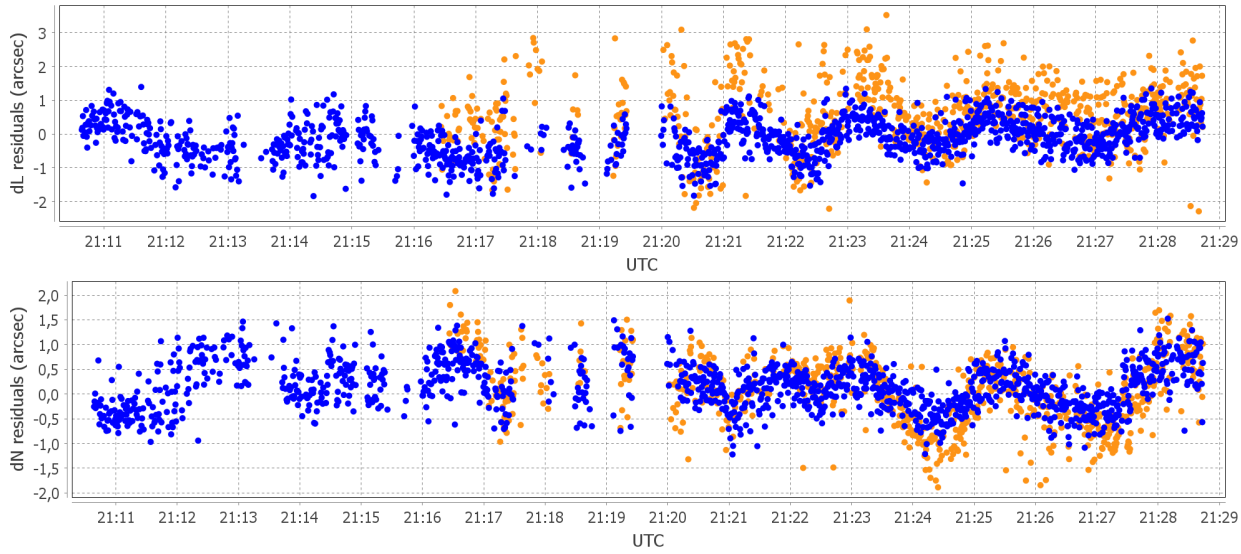

Fig. 6.6 – Differences between astrometric measurements and ILRS orbital product during Lageos-1 passage on 03 Aug 2022 at PST3e telescope. The blue points are the PSST measurements, and the orange points are the LEMUR measurement.

The cases presented in Fig. 6.4 and 6.6 illustrate how image processing can be complex when using a fast focal ratio optical system. We considered a small observation set, but even in this case, we found several examples with clearly expressed systematic measurement biases caused by the image processing methods and the images' features.
The usually used procedure of obtaining a short astrometric observation series, as a rule, does not allow us to detect and study systematic measurement biases. Even in those rare cases when systematic measurement biases are detected in short observation series, there is no way to interpret the causes of their genesis in practice. On the one hand, this situation forces observation analysis centers to consider systematic measurement biases as part of the random measurement error and, on the other hand, does not give observation providers an understanding of which observation features, or observation processing should be focused on for improving the measurement quality.

6.3 GPS and GSO objects

As an example of high-orbit objects (orbit altitude above 6000 km), we used objects from the GPS constellation and several objects in geostationary (GEO) and geosynchronous (GSO) orbits. All these objects require similar observation methods and a similar image processing technique. Therefore, we will consider the results for these objects together. In total, we obtained nine passes for these objects (Table 6.1).

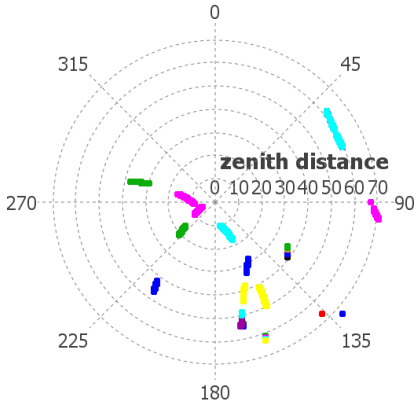

Fig. 6.7 – The location of MEO and GSO objects' observation sub-series on the celestial sphere. Each sub-series in each pass is marked with its color. The colors of the sub-series in different passes may be repeated.

For our analysis, we divided each spacecraft pass into several sub-series, which approximately cover the original continuous observation series (Fig. 6.7). Each sub-series contains 100 or more measurements, which allows us to

obtain sufficiently reliable estimates of the standard deviation of one measurement for each sub-series, as well as to estimate the sub-series bias (mean of sub-series O-Cs) and standard deviation.

Fig. 6.8 shows the dependence of the standard deviation of one measurement in a sub-series on the average elevation of observations in each sub-series. It is clear that the object's elevation is a significant factor affecting the accuracy of one measurement when an object is below 30 degrees over the horizon. It is also visible that the precision of PSST measurements along the trail is better than that of LEMUR measurements in the case of PST3c telescope observations. In all other cases, the precision of one measurement for both pipelines is similar.

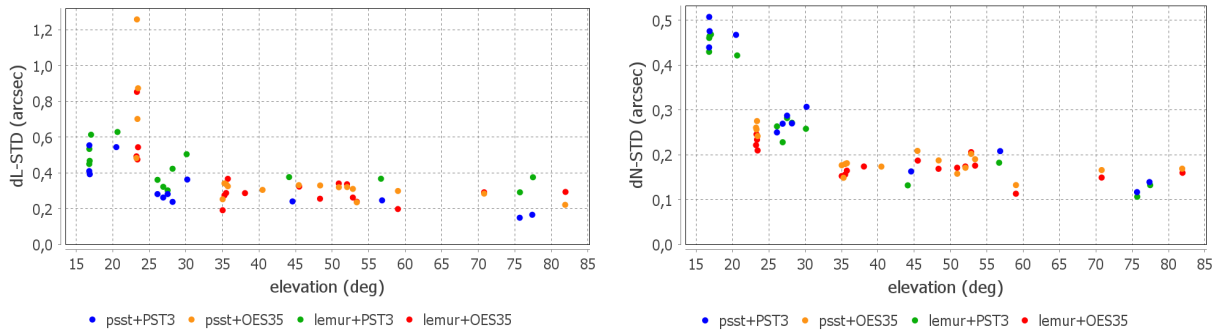

(a) (b)

Fig. 6.8 – The standard deviation of one measurement in a sub-series with respect to the average elevation of observations in each sub-series. Fig. (a) shows the standard deviation of the L-component of O-Cs, and fig. (b) shows the standard deviation of the N-component of O-Cs. The color marks the different pairs of telescopes and image-processing pipelines.

Fig. 6.9 shows that

1) All sub-series have a significant bias with respect to the reference orbit. The bias values can reach several tenths of an arcsecond when the standard deviation of one measurement is in the interval from 0.2” to 0.5”.
2) The PSST and LEMUR pipelines produce results with systematic difference which can reach 0.2”.

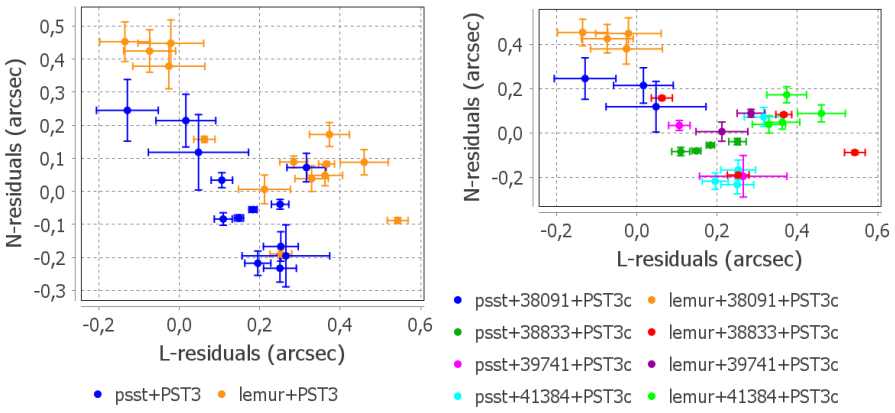

(a) (b)

Fig. 6.9 – The mean values of the sub-series O-Cs with 3σ uncertainties for objects on high orbits (orbit altitude greater than 6000km) observed with the PST3c telescope. The colors in Fig. a) show different pipelines. The colors in Fig. b) show different pairs of object passes and processing pipelines.

The graph in Fig. 6.10 displays the O-C's average values for MEO and GSO object observations made on the OES35 telescope. Unlike the observations on the PST3c telescope (Fig. 6.9), we do not notice any significant biases between the sub-series mean values of O-Cs obtained from processing observations using different pipelines. This result indicates that the PSST pipeline is more adaptable to observations from different sources than the LEMUR. However, we do observe significant biases (around one or several tenth arcseconds) in the O-C's mean values obtained from both telescopes relative to reference orbits. These angular bias magnitudes of the measurement series are around several tens of meters in terms of object space position biases. These biases may be due to inaccuracies in image

processing or in the method used for comparing measurements and reference orbits. The small bias magnitude, the limited number of observations, and the observed track assortment do not allow us to draw unambiguous conclusions on this issue, and further investigation is required. Notably, the biases in the measurement series of IRNSS objects were greater than those for the rest of the objects we considered in high orbits. This result probably indicates lower accuracy of orbital predictions for IRNSS objects.

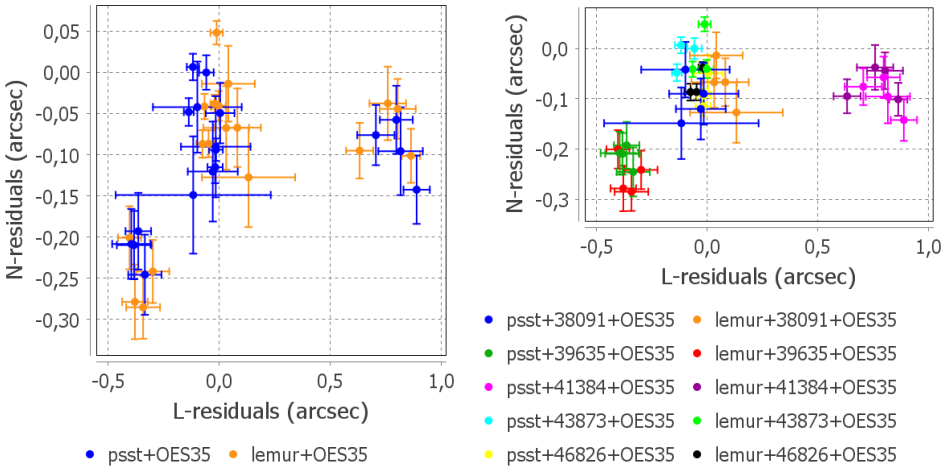

(a) (b)

Fig. 6.10 – The mean values of the sub-series O-Cs with 3σ uncertainties for objects on high orbits (orbit altitude greater than 6000km) observed with the OES35 telescope. The colors in Fig. a) show different pipelines. The colors in Fig. b) show different pairs of object passes and processing pipelines.

7. CONCLUSIONS

In this work, we conducted the detailed accuracy analysis of astrometric measurements of RSOs using the LEMUR and PSST pipelines across three telescopes on the same observation data sets. We identified factors that contribute to deviations between the measurements and reference orbit. Our research highlights three main factors that cause deviations between the measurements and reference orbit.

1. The comparison procedures themselves can be inaccurate, leading to systematic deviations of measured coordinates of RSOs from the reference orbit.
2. The measurement procedures provided by the image processing pipelines can result in systematic biases in measurements.
3. The orbit ephemeris inaccuracy can lead to systematic O-C deviations.

In order to reduce the contribution of systematic errors during the comparison procedure, in addition to the standard actions of excluding the aberrations and correction of the measurement time biases, we

1) corrected the observation site location coordinates,
2) corrected the refraction parallax effect,
3) excluded ILRS orbits from consideration, the accuracy of which was in doubt.

We showed that

1. The LEMUR and PSST pipelines can accurately process images from various equipment. Both pipelines have similar accuracy for all types of objects. Both pipelines measure RSO coordinates with sub-pixel accuracy. The accuracy of one measurement of the coordinates of LEO objects is about one arcsecond; for objects on medium and high orbits, the accuracy is about a few tenths of an arcsecond. This meets the modern requirements for the accuracy of astrometric measurements of such objects and is not inferior to the accuracy of measurements achieved by other researchers. [4, 5, 6].
2. Images from the fast (f/1.0) PST3e telescope are a challenge for measuring the RSO coordinates for both pipelines. We have shown some examples (e.g. Fig. 6.6) that a local sequential group of measurements can have a significant systematic bias with a magnitude larger than the RMS value of one measurement. These results show that the evaluation of quality of measurements obtained on telescopes with fast focal ratios requires more careful studies than single RMS estimates for selected observation cases.

3. The PSST pipeline produces more accurate measurements of the RSO coordinates than the LEMUR pipeline on images from the PST3e telescope.
4. The accuracy of a single measurement of both pipelines depends on many factors and has significant variations depending on the image characteristics. In some cases, the PSST pipeline has better accuracy, in others, LEMUR.
5. The LEMUR and the PSST pipelines often produce a comparable number of measurements for the same observation data sets. But sometimes, the LEMUR makes 1.5 or more times larger number of measurements than the PSST, which can be important in the case of a short observation series.
6. The accuracy of a single measurement of the coordinates of MEO and GSO objects at a zenith distance greater than 60° is primarily determined by the atmosphere conditions.
7. We showed that the mean residue of measured astrometric positions from both pipelines with respect to the reference orbit can have significant systematic bias. The typical value of a single measurement series bias is at the level of tenths of an arcsecond. In all cases we considered, the bias was below 1 arcsecond, even for LEO objects. Thus, we have shown the possibility of achieving the measurement accuracy of the RSO coordinates better than 1 arcsecond on all types of orbits.
8. In almost all cases we considered, the measurement results of the PSST and LEMUR pipelines had a significant systematic bias with respect to each other (see Figures 6.3, 6.5, and 6.9). The differences between the biases of the measurement series produced by PSST and LEMUR pipelines for the same observation series are of the same order of magnitude as the biases of the measurement series relative to the reference orbits.

7. REFERENCES

[1] Kamiński K. et al. New Optical Sensors Cluster for Efficient Space Surveillance and Tracking. *Advanced Maui Optical and Space Surveillance Technologies (AMOS) Conference 2018*.

[2] Kozhukhov O.M. et al. New Two-Tubes Telescope for Observation of Near-Earth Space. *Advanced Maui Optical and Space Surveillance Technologies (AMOS) Conference 2022*.

[3] Savanevych V.E. et al. CoLiTecVS software for the automated reduction of photometric observations in CCD-frames. *Astronomy and Computing*. **40**, 100605, 2022. DOI:/10.1016/j.ascom.2022.100605

[4] Choi J. et al. Optical Tracking Data Validation and Orbit Estimation for Sparse Observations of Satellites by the OWL-Net. *Sensors*. **18**, 6, 1868, 2018. DOI:/10.3390/s18061868.

[5] Jilete B. et al. Optical observations in ESASSA programme. *Revista Mexicana de Astronomía y Astrofísica Serie de Conferencias*. **51**, 139–143, 2019. DOI:/10.22201/ia.14052059p.2019.51.24.

[6] Silha J. et al. AGO70: passive optical system to support SLR tracking of space debris on LEO. In*: 22nd Advanced Maui Optical and Space Surveillance Technologies (AMOS) Conference 2021*.

[7] Labriji H., Herscovici-Schiller O., Cassaing F. Computation of the lateral shift due to atmospheric refraction. *Astronomy & Astrophysics*. 662, A61, 2022. DOI:/10.1051/0004-6361/202142338.

[8] Najder J., Sośnica K.. Quality of Orbit Predictions for Satellites Tracked by SLR Stations. *Remote Sensing*. **13**, 7, 1377, 2021. DOI:/10.3390/rs13071377.

[9] Shakun L.S. Features of Kotlin Orbit Estimation Library. *Odessa Astronomical Publications*. **31**, 191–195, 2018. DOI:/10.18524/1810-4215.2018.31.145962.

[10] ORbit Extrapolation KIT (Orekit) https://www.orekit.org/ Online; Accessed: 30.08.2023

[11] Java implementation of "Standards Of Fundamental Astronomy" (JSOFA) http://javastro.github.io/jsofa/ Online; Accessed: 30.08.2023